Rotational and spin viscosities of water: Application to nanofluidics

J. S. Hansen,[1,a)] Henrik Bruus,[2,b)] B. D. Todd,[3,c)] and Peter J. Daivis[4,d)]
[1]*Department of Sciences, DNRF Centre "Glass and Time" IMFUFA, Roskilde University, P.O. Box 260, Roskilde DK-4000, Denmark*
[2]*Department of Micro- and Nanotechnology, Technical University of Denmark, DTU Nanotech Building 345 East, Kongens Lyngby DK-2800, Denmark*
[3]*Centre for Molecular Simulation, Swinburne University of Technology, P.O. Box 218, Hawthorn, Victoria 3122, Australia*
[4]*Applied Physics, School of Applied Sciences, RMIT University, G.P.O. Box 2476, Melbourne, Victoria 3001, Australia*

(Received 11 June 2010; accepted 28 August 2010; published online 11 October 2010)

In this paper we evaluate the rotational viscosity and the two spin viscosities for liquid water using equilibrium molecular dynamics. Water is modeled via the flexible SPC/Fw model where the Coulomb interactions are calculated via the Wolf method which enables the long simulation times required. We find that the rotational viscosity is independent of the temperature in the range from 284 to 319 K. The two spin viscosities, on the other hand, decrease with increasing temperature and are found to be two orders of magnitude larger than that estimated by Bonthuis *et al.* [Phys. Rev. Lett. **103**, 144503 (2009)] We apply the results from molecular dynamics simulations to the extended Navier–Stokes equations that include the coupling between intrinsic angular momentum and linear momentum. For a flow driven by an external field the coupling will reduce the flow rate significantly for nanoscale geometries. The coupling also enables conversion of rotational electrical energy into fluid linear momentum and we find that in order to obtain measurable flow rates the electrical field strength must be in the order of 0.1 MV m^{-1} and rotate with a frequency of more than 100 MHz. © *2010 American Institute of Physics*. [doi:10.1063/1.3490664]

I. INTRODUCTION

In the fluid dynamical description of macroscopic systems the coupling of the fluid's molecular details to the hydrodynamical degrees of freedom are usually disregarded because the former can often safely be ignored. However, this coupling does exist[1–3] and recently Hansen *et al.*[4–6] and Bonthuis *et al.*[7] showed via molecular dynamics that the coupling between the molecular intrinsic angular momentum and the fluid translational motion can become important on small length scales. Hansen *et al.*[4–6] studied simple flows of fluids composed of linear molecules, such as low density alkenes, and concluded that for such systems the flow rate is significantly reduced for confinements of the order of 10 nm. In their very interesting work Bonthuis *et al.*[7] showed that by applying a rotational electrical field to a system composed of molecules with an electrical dipole moment the molecular intrinsic angular momentum can be converted into translational motion. This conversion is most effective on small length scales due to the large field strengths required.

To include the molecular intrinsic angular momentum into the fluid dynamical description, one needs a total of four phenomenological coefficients for an incompressible isotropic fluid: (i) the shear viscosity, (ii) the rotational viscosity, and [(iii) and (iv)] the two spin viscosities. These coefficients are defined via the corresponding linear constitutive relations. For a fluid composed of uniaxial molecules the rotational viscosity η_r is given via[2,3]

$$\mathbf{P}^d = -\eta_r(\boldsymbol{\nabla}\times\mathbf{u} - 2\boldsymbol{\Omega}), \tag{1}$$

where $\mathbf{P}^d$ is the vector dual of the antisymmetric part of the pressure tensor, $\mathbf{u}$ is the velocity field, and $\boldsymbol{\Omega}$ is the angular velocity field. The rotational viscosity thus describes the decay of the antisymmetric stress: this process is a fast local process and originates from molecular intrinsic angular momentum relaxation. The spin viscosities ζ_0 and ζ_r are in general given by the relations[8]

$$\mathsf{Q}^{os} = -2\zeta_0(\boldsymbol{\nabla}\boldsymbol{\Omega})^{os} \quad \text{and} \quad \mathbf{Q}^d = -\zeta_r(\boldsymbol{\nabla}\times\boldsymbol{\Omega}). \tag{2}$$

Here Q^{os} is the traceless symmetric part of the couple tensor and $\mathbf{Q}^d$ is the vector dual of the antisymmetric part of the couple tensor. The spin viscosities are both related to angular momentum diffusion.[6,8]

In the work by Bonthuis *et al.*[7] the authors estimated the sum of the two spin viscosities to be $(\zeta_0+\zeta_r)=a^2\eta_r$, where a is the diameter of the water molecule. However, this scaling law is not likely to be very accurate and will significantly effect the prediction of the coupling between the microscopic and hydrodynamical degrees of freedom.[9] In this paper we calculate the rotational and spin viscosities of water at different temperatures using equilibrium molecular dynamics (EMD) simulations. The EMD data show orders of magnitude difference with the scaling law used by Bonthuis *et al.* We then insert the calculated values of the viscosities in the extended Navier–Stokes equations that include the molecular

a)Electronic mail: jesperschmidthansen@gmail.com.
b)Electronic mail: bruus@nanotech.dtu.dk.
c)Electronic mail: btodd@swin.edu.au.
d)Electronic mail: peter.daivis@rmit.edu.au.

TABLE I. Parameter values, self-diffusivity, and shear viscosity for the rigid and flexible SPC models using the PME and Wolf methods. For this work the density is 994.61 kg m^{-3} and pressure is around 49 MPa, which is close to the SPC model pressure (Ref. 14). The uncertainties are standard errors.

	k_s (kJ mol^{-1} nm^{-2})	k_θ (kJ mol^{-1} rad^{-2})	l_b (nm)	θ_0 (rad)	α_w (nm^{-1})	U at 300 K (kJ mol^{-1})	D at 298.16 K (10^{-9} m^2 s^{-1})	η_0 at 300.2 K (10^{-3} Pa s)
SPC/Fw (Wolf)[a]	7047.7	317.78	0.1	1.97	1.896	−39.52	2.68 ± 0.01	0.67 ± 0.03
SPC (PME)[b]	⋯	⋯	0.1	1.911	⋯	−41.69	4.02	0.4
SPC/Fw (PME)[c]	7028.4	317.78	0.101	1.976	⋯	⋯	2.35	0.75
Experiment[d]	⋯	⋯	0.097	1.83	⋯	⋯	2.3	0.85

[a]This work.
[b]References 10, 13, and 14.
[c]Reference 10.
[d]References 15 and 16.

intrinsic angular momentum and analyze two simple nanofluidic flows, namely, a planar Poiseuille flow and a flow generated by a rotating electrical field.

The paper is organized as follows. In the next section we present the applied water model and it will be explained how the viscosities are calculated. In Sec. III we present the results and in Sec. IV we discuss the two different flows. The final section is devoted to conclusions.

II. METHOD

The water molecules are modeled via the SPC/Fw model.[10] Compared to the rigid SPC, SPC/E, TIP3P, and TIP4P models, this model predicts several quantities more accurately, for example, self-diffusivity, shear viscosity, and the critical point.[10,11] The SPC/Fw model is a flexible three-site model that allows for the hydrogen-oxygen covalent bond to vibrate as well as bond bending. Thus, the potential energy for the system can be written as

$$U = \sum_{\text{pairs}} U_{\text{LJ}}(r_{i\alpha j\beta}) + \sum_{\text{bonds}} U_b(r_{i\alpha i\beta}) + \sum_{\text{angles}} U_a(\theta_i) + \sum_{\text{pairs}} U_C(r_{i\alpha j\beta}), \tag{3}$$

where $r_{i\alpha j\beta}$ is the distance between atom α in molecule i and atom β in molecule j, and θ_i is the bond angle in water molecule i. The pair potential, U_{LJ}, is given by the truncated and shifted Lennard-Jones potential

$$U_{\text{LJ}}(r_{i\alpha j\beta}) = 4\epsilon\left[\left(\frac{\sigma}{r_{i\alpha j\beta}}\right)^{12} - \left(\frac{\sigma}{r_{i\alpha j\beta}}\right)^{6}\right] - U(r_c) \quad \text{if } r_{i\alpha j\beta} \le r_c. \tag{4}$$

Here σ is a length scale, ϵ is an energy scale, $r_c = 2.844\sigma$ is the critical cutoff, and $U(r_c)$ is the unshifted potential. It is only the oxygen atoms that interact via the Lennard-Jones potential. The bond stretching potential between the hydrogen and oxygen atoms is given by the harmonic spring potential

$$U_b(r_{i\alpha i\beta}) = \tfrac{1}{2}k_s(r_{i\alpha i\beta} - l_b)^2, \tag{5}$$

where k_s is the spring constant and l_b is the zero-force (or equilibrium) bond length. The bending potential will here be given by the asymmetric potential

$$U_a(\theta_i) = \tfrac{1}{2}k_\theta(\cos\,\theta_i - \cos\,\theta_0)^2, \tag{6}$$

where k_θ is the force bending constant and θ_0 is the equilibrium bending angle. To account for the Coulomb potential we have applied the Wolf approximation method[12,13] which enables one to carry out the necessary long simulation runs. The damped Wolf potential for charge neutral molecules without intramolecular Coulomb interactions reads[13]

$$U_C(r_{i\alpha j\beta}) = z_{i\alpha}z_{j\beta}\left[\frac{\text{erfc}(\alpha_w r_{i\alpha j\beta})}{r_{i\alpha j\beta}^2} - \left(\frac{\text{erfc}(\alpha_w r_c)}{r_c} + \frac{2\alpha_w}{\sqrt{\pi}}\exp(-(\alpha_w r_c)^2)\right)\left(\frac{r_{i\alpha j\beta}}{r_c} - 1\right)\right], \tag{7}$$

if $r_{i\alpha j\beta} \le r_c$ and where α_w is the damping parameter and $z_{i\alpha}$ is the partial atomic charge. We use $z = -0.82e$ and $z = 0.41e$ for oxygen and hydrogen, respectively, e being the elementary charge. Table I lists the different parameter values.

The systems were prepared by compressing a very dilute gas composed of 243 water molecules into a liquid with the desired density while the equations of motion were integrated forward in time using a leap-frog integration scheme[17] with a time step of 0.8314 fs. The simulations were carried out in the NVT-ensemble via an atomic Nosé–Hoover thermostat.[18,19] After equilibration the molecular pressure tensor P and couple tensor Q were calculated in order to evaluate the transport coefficients. The microscopic expressions for the tensors and the corresponding equations for the transport coefficients are given by Evans *et al.*,[8,20] however, since this may not be common knowledge we will here briefly state the important results. The Irving–Kirkwood definition of the molecular pressure tensor is[21]

$$\mathsf{P} = \frac{1}{V}\left[\sum_i \frac{\mathbf{p}_i\mathbf{p}_i}{m_i} + \sum_i \sum_{j>i} \mathbf{r}_{ij}\mathbf{F}_{ij}\right], \tag{8}$$

where V is the system volume, $\mathbf{p}_i$ is the center of mass momentum of molecule i, $\mathbf{r}_{ij} = \mathbf{r}_i - \mathbf{r}_j$, where $\mathbf{r}_i$ is the center of mass of i, and m_i is the mass of i. $\mathbf{F}_{ij}$ is the force acting on molecule i due to j and is given by $\mathbf{F}_{ij} = \Sigma_{i\alpha}\Sigma_{j\beta}\mathbf{F}_{i\alpha j\beta}$, where $\mathbf{F}_{i\alpha j\beta}$ is the force between atom α in molecule i and atom β in molecule j. The couple tensor is given by[8]

$$\mathsf{Q} = \frac{1}{V}\left[\sum_i \mathbf{p}_i\mathbf{s}_i + \sum_i \sum_{j>i} \mathbf{r}_{ij}\mathbf{\Gamma}_{ij}\right]. \tag{9}$$

Here $\mathbf{s}_i$ is the angular momentum of molecule i and $\mathbf{\Gamma}_{ij}$ is the torque on i due to j, i.e.,

$$\mathbf{s}_i = \frac{1}{m_i}\sum_{i\alpha} m_{i\alpha}\mathbf{R}_{i\alpha} \times \mathbf{v}_{i\alpha}$$

and

$$\mathbf{\Gamma}_{ij} = \sum_{i\alpha}\left[\mathbf{R}_{i\alpha} \times \sum_{j\beta} \mathbf{F}_{i\alpha j\beta}\right], \tag{10}$$

where $\mathbf{R}_{i\alpha}=\mathbf{r}_{i\alpha}-\mathbf{r}_i$ and $m_{i\alpha}$ and $\mathbf{v}_{i\alpha}$ are the mass and velocity of atom α in molecule i, respectively. To evaluate the rotational and spin viscosities the pressure tensor and the couple tensor are decomposed into traceless symmetric and antisymmetric parts

$$\mathsf{P}^a = \tfrac{1}{2}(\mathsf{P}-\mathsf{P}^T),\quad \mathsf{Q}^{os} = \tfrac{1}{2}(\mathsf{Q}+\mathsf{Q}^T) - \tfrac{1}{3}\mathrm{tr}(\mathsf{Q})$$

and

$$\mathsf{Q}^a = \tfrac{1}{2}(\mathsf{Q}-\mathsf{Q}^T), \tag{11}$$

where superscript T denotes the transpose of the tensor and $\mathrm{tr}(\mathsf{Q})$ is the trace of Q. From P and Q one can alternatively obtain the dual vectors of the antisymmetric parts via the Levi–Civita tensor $\boldsymbol{\epsilon}$, e.g., for the pressure tensor

$$\mathbf{P}^d = \tfrac{1}{2}\boldsymbol{\epsilon}:\mathsf{P}^T = (P^a_{(yz)}, P^a_{(zx)}, P^a_{(xy)}). \tag{12}$$

From the pressure and couple tensors it is possible to calculate the rotational and spin viscosities. Evans and Hanley[20] pointed out that the rotational viscosity cannot be expressed via a Green–Kubo relation, because it describes a wave-vector independent process, namely, the relaxation of molecular intrinsic angular momentum. It can, however, be found by solving the generalized Langevin equation.[22] Evans and Hanley[20] also showed that the Laplace transform of the rotational viscosity kernel, $\tilde{\eta}_r(s)$, for fluids composed of linear molecules is given by

$$\tilde{\eta}_r(s) = \frac{\tilde{C}_{\eta_r}(s)}{1 - \dfrac{4}{\rho I}\dfrac{\tilde{C}_{\eta_r}(s)}{s}}, \tag{13}$$

where ρ is the density, I is the molecular moment of inertia per unit mass, and $\tilde{C}_{\eta_r}(s)$ is the Laplace transform

$$\tilde{C}_{\eta_r}(s) = \frac{V}{k_BT}\int_0^\infty e^{-st} C_{\eta_r}(t)dt, \tag{14}$$

$C_{\eta_r}(t)$ is the autocorrelation function (ACF) of the antisymmetric part of the pressure tensor

$$C_{\eta_r}(t) = \frac{1}{3}\sum_{(ij)} \langle P^a_{(ij)}(0)P^a_{(ij)}(t)\rangle. \tag{15}$$

Here the sum runs over the (xy), (xz), and (yz) off-diagonal tensor elements. Equation (13) is not particularly useful since there exists a singularity for $4\tilde{C}_{\eta_r}(s)/(\rho I s)=1$. Evans and Hanley therefore suggested to invert the problem by expressing $\tilde{C}_{\eta_r}(s)$ in terms of $\tilde{\eta}_r(s)$,

$$\tilde{C}_{\eta_r}(s) = \frac{s\tilde{\eta}_r(s)}{s + \dfrac{4}{\rho I}\tilde{\eta}_r(s)}. \tag{16}$$

By proposing a functional form for $\tilde{\eta}_r(s)$ is then possible to fit Eq. (16) to EMD data and thereby extract the rotational viscosity. We will do so in Sec. III. The spin viscosities are given directly via the Green–Kubo integral[8]

$$\zeta_0 = \frac{V}{k_BT}\int_0^\infty \frac{1}{3}\sum_{(ij)} \langle Q^{os}_{(ij)}(0)Q^{os}_{(ij)}(t)\rangle dt, \tag{17a}$$

$$\zeta_r = \frac{V}{k_BT}\int_0^\infty \frac{1}{3}\sum_{(ij)} \langle Q^{a}_{(ij)}(0)Q^{a}_{(ij)}(t)\rangle dt. \tag{17b}$$

Again, the sums run over the (xy), (xz), and (yz) elements.[23,24] We will denote the ACFs under the integrals $C_{\zeta_0}(t)$ and $C_{\zeta_r}(t)$, respectively.

After the equilibration phase, the ACFs were sampled over a time span of 17 ps. For each temperature 900 samples were taken giving around 20×10^6 time steps per state point. On an Intel 2.4 GHz CPU this took approximately six days.

III. RESULTS

Since we have applied a slightly different method to evaluate the angle bending forces and the Coulomb interaction, we first compare the total potential energy, self-diffusivity, and shear viscosity with previously published data. Table I shows the comparison with EMD simulations where the Coulomb interactions are computed via the particle mesh Ewald (PME) method. In this work, the self-diffusivity and shear viscosity are found from the standard Green–Kubo integral. It is seen that the SPC/Fw model predicts the diffusivity and shear viscosity far better than the classical SPC model. The PME method is slightly better to predict the fluid properties than the Wolf approximation, however, this method requires longer simulation times in order to obtain reliable values of the spin viscosities due to the slow convergence of the integrals in Eq. (17). It is worth mentioning that the extended SPC model, SPC/E, yields approximately the same values for the shear viscosity using the PME method as the SPC/Fw (Wolf) model.[10] We also refer the reader to Gonzáles and Abascal[25] where it is shown that the TIP4P/2005 model is in very good agreement with experimental data of the viscosity for three different temperatures. However, to our knowledge no extensive comparison of different transport properties has been made between the SPC/Fw and the TIP4P/2005 water models, i.e., it cannot yet be concluded which one of these perform the best.

The ACFs for the antisymmetric part of pressure tensor, $C_{\eta_r}(t)$, the symmetric part of the couple tensor, $C_{\zeta_0}(t)$, and antisymmetric part of the couple tensor, $C_{\zeta_r}(t)$, are plotted in Fig. 1(a) as functions of time for $T=292.4$ K. As noted earlier, $C_{\zeta_0}(t)$ and $C_{\zeta_r}(t)$ have long decay times compared to $C_{\eta_r}(t)$; we have found the decay time to be around 16–17 ps for $T=284$ K, which is the lowest temperature in this work.

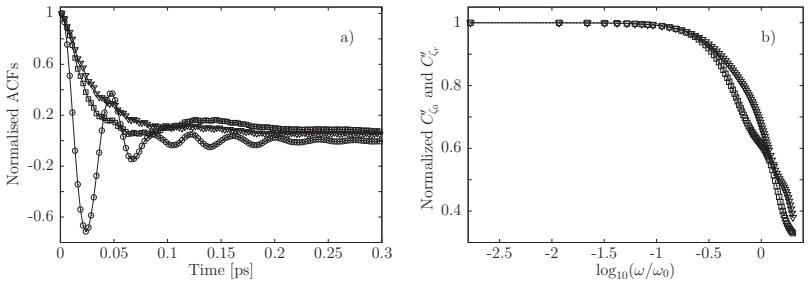

FIG. 1. (a) Normalized ACFs of the antisymmetric part of the pressure tensor (circles), the symmetric part of the couple tensor (squares), and the antisymmetric part of the couple tensor (triangles). Only short time behavior is shown. The lines serve as guide to the eyes. (b) Normalized real part of the Fourier transform of the symmetric part of the couple tensor (squares) and the antisymmetric part of the couple tensor (triangles) as functions of frequency. $\omega_0=600$ GHz. The lines serve as guide to the eyes. For both (a) and (b) the temperature is 292.4 K.

The frequency dependence of the spin viscosities can be found from the one-sided Fourier transform (or complex viscosities). For example, the transform of $C_{\zeta_0}(t)$ is written as

$$C^*_{\zeta_0}(\omega) = C'_{\zeta_0}(\omega) + iC''_{\zeta_0}(\omega) = \int_0^\infty C_{\zeta_0}(t)e^{-i\omega t}dt, \tag{18}$$

where $C'_{\zeta_0}(\omega)$ and $C''_{\zeta_0}(\omega)$ are the real and imaginary parts of the complex spin viscosity. To remove the effect of the truncation of the ACFs and the poor signal to noise ratio at large times the data are smoothed with a Hann window[26] before Fourier transforming. In Fig. 1(b) the real part of the complex spin viscosities have been plotted as functions of frequency. It is observed that the viscoelastic response (as manifested in angular momentum fluxes) appears around 60 GHz. This is also where the shear viscosity shows a viscoelastic response.

Evans and Hanley[20] assumed a Lorentzian type functional form for the rotational viscosity in Laplace space, namely,

$$\tilde{\eta}_r(s) = \frac{\eta_r}{1+s\tau}, \tag{19}$$

where $\eta_r = \tilde{\eta}_r(0)$ and τ is the relaxation time. This expression is actually closely related to the Maxwell model for the frequency dependent viscosity. Substituting this into Eq. (16) one obtains

$$\tilde{C}_{\eta_r}(s) = \frac{\eta_r s}{4\eta_r/\rho I + s + \tau s^2}. \tag{20}$$

To find η_r one can fit Eq. (20) to the Laplace transformed simulation data for $C_{\eta_r}(t)$, however, as stated above this is only strictly valid for linear molecules where I is given by the principle moment of inertia per unit mass, I_p, as $I=2I_p/3$. Water is not a linear molecule, but we will assume that it can be treated as approximately linear with an effective principle moment of inertia I_p. This quantity can be found by Taylor expanding Eq. (20) around $s=0$

$$\tilde{C}_{\eta_r}(s) = \frac{1}{4}\rho I s + \frac{1}{16}\frac{\rho^2}{\eta_r}s^2 + O(s^3). \tag{21}$$

The first order coefficient can be calculated directly from simulation data, i.e., in the limit of $s \to 0$ we obtain $I = 4\tilde{C}'(s)/\rho$. The apparent moment of inertia per unit mass is found to be 8.4×10^{-22} m^2. For comparison, if one approximates the water molecule to be a linear molecule, i.e., with a bonding angle of 180°, the moment of inertia is 8.33×10^{-22} m^2. Bertolini and Tani[27] found the relaxation time $\tau=0.08$ ps which we will use throughout. Figure 2 compares the least squares fit of Eq. (20) using only η_r as fitting parameter to the Laplace transformed data for $C_{\eta_r}(t)$. As it can be seen, the fit shows good agreement over a large range of s. It should be noted that many other functional forms for $\tilde{\eta}_r(s)$ have been tested without improving the fit.

Table II summarizes the main results from the EMD simulations. It is seen that the rotational viscosity does not vary significantly in the temperature range studied here, that is, the relaxation of angular momentum into linear momentum is temperature independent in this interval. Since the shear viscosity decreases with temperature the rule-of-thumb stating that the ratio between the rotational and shear viscosities around 0.1[20,27] is indeed compromised for higher temperatures. The spin viscosities decrease with respect to temperature which is likely due to the less cohesive state of the fluid for higher temperatures as is the case for the shear viscosity. The temperature dependence of the spin viscosities has been found to fit both a linear and (weak) exponential function well and additional data are needed in order to establish an exact empirical functional dependence. It is also noted that the spin viscosities are around two orders of magnitude larger than the value used by Bonthuis *et al.*,[7] which is an important result, because this will increase the effect from the coupling between the angular momentum and the fluid linear momentum considerably. We stress that Bonthuis *et al.* use a simple scaling law that relates the spin viscosities with the rotational viscosity. While the assumption seems reasonable at first, there is no theoretical or empirical justification for this relation. Recall, the rotational viscosity and the spin viscosities describe two different phenomena. According to our knowledge this work is the first to evaluate the spin viscosities of water directly, and without any assumptions,

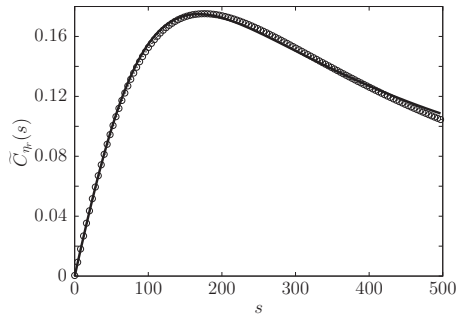

FIG. 2. Least squares fit (full line) of Eq. (20) to the Laplace transformed simulation data of C_{η_r} (circles). In this fit $\eta_r=1.7\times10^{-4}$ Pa s. $\tau=0.08$ ps and $I=8.4\times10^{-22}$ m^2 as discussed in the text. The temperature is $T=292.4$ K.

TABLE II. The rotational and spin viscosities for different temperatures at density of 994.61 kg m^{-3}. The last column shows the ratio between the rotational and shear viscosity. The uncertainties are standard errors. We note that for TIP4P Bertolini and Tani (Ref. 27) find $\eta_r=0.19\pm0.04\times10^{-3}$ Pa s at $T=245$ K and $T=298$ K.

T (K)	η_0 (10^{-3} Pa s)	η_r (10^{-3} Pa s)	ζ_0 (10^{-21} kg m s^{-1})	ζ_r (10^{-21} kg m s^{-1})	η_r/η_0
284	0.92 ± 0.09	0.17 ± 0.03	1.4 ± 0.1	1.6 ± 0.2	0.19
289	0.83 ± 0.09	0.17 ± 0.02	1.2 ± 0.1	1.5 ± 0.2	0.20
293	0.76 ± 0.04	0.17 ± 0.02	1.2 ± 0.2	1.4 ± 0.1	0.22
299	0.7 ± 0.1	0.17 ± 0.03	0.9 ± 0.1	1.2 ± 0.2	0.24
305	0.61 ± 0.05	0.16 ± 0.04	0.93 ± 0.09	1.2 ± 0.2	0.27
309	0.56 ± 0.08	0.164 ± 0.003	0.83 ± 0.07	1.0 ± 0.2	0.29
313	0.54 ± 0.06	0.161 ± 0.001	0.8 ± 0.1	0.9 ± 0.1	0.29
319	0.48 ± 0.04	0.160 ± 0.002	0.7 ± 0.1	0.92 ± 0.08	0.33

using the Green–Kubo formalism. It is therefore not possible to do any detailed comparison of the data with previous published results.

IV. APPLICATION: WATER FLOW IN NANOCHANNELS

Having evaluated the relevant transport coefficients it is possible to quantitatively analyze the effects of molecular rotation on the fluid velocity field. In this section we will study two different systems where water is confined in a nanoslit pore: (i) one in which the water flows through the pore due to an external constant gradient force (like pressure driven planar Poiseuille flow) and (ii) one where a rotating homogeneous electrical field is applied to the system. The latter situation has been discussed by Bonthuis *et al.*,[7] however, in their analysis they used different values of the rotational and spin viscosities.

A. Flow reduction in a planar Poiseuille flow

Consider a fluid confined between parallel walls located at $\pm h$ with $h>0$ such that the z direction is the only direction of confinement and the walls are infinite in extent in the (x,y)-plane. The water molecules are assumed to be uniaxial with apparent moment of inertia per unit mass I, as discussed above in Sec. III. The fluid may be subjected to a constant external force F_e per unit mass in the x direction and constant torque Γ_y per unit mass normal to the (x,z)-plane. If F_e and Γ_y are sufficiently small the extended Navier–Stokes equations read[8]

$$\rho\frac{\partial u_x}{\partial t}=\rho F_e+(\eta_0+\eta_r)\frac{\partial^2 u_x}{\partial z^2}-2\eta_r\frac{\partial \Omega_y}{\partial z}, \tag{22a}$$

$$\rho I\frac{\partial \Omega_y}{\partial t}=\rho\Gamma_y+2\eta_r\left(\frac{\partial u_x}{\partial z}-2\Omega_y\right)+\zeta\frac{\partial^2\Omega_y}{\partial z^2}, \tag{22b}$$

where u_x is the x vector element of the streaming velocity field, Ω_y is y vector element of the angular velocity field, and $\zeta=\zeta_0+\zeta_r$.

In the case where $\Gamma_y=0$ and where the no-slip boundary conditions are applied, i.e., $u_x(\pm h)=\Omega_y(\pm h)=0$, Eq. (22) can be solved analytically.[28] Furthermore, it has been shown that the relative flow rate reduction due to internal molecular rotation is given by[29]

$$1-\frac{Q}{Q^P}=-\frac{3\eta_r(\tanh(Kh)-Kh)}{\tanh(Kh)(\eta_0+\eta_r)(Kh)^2}, \tag{23}$$

where $K=\sqrt{4\eta_r\eta_0/(\eta_0+\eta_r)\zeta}$ and Q^P and Q are the flow rates for $\eta_r\neq0$ and $\eta_r=0$, respectively, i.e., when the coupling is included and when it is ignored. Equation (23) is plotted in Fig. 3 as a function of pore width for water. It can be seen that there exists a surprisingly large flow reduction for small pore widths. This means that the coupling between the molecular rotation and the hydrodynamical degrees of freedom must be considered to give a correct prediction of the flow rate on these length scales. This result is also valid for nonzero slip length.

B. Flow generation

In the next scenario we let a uniform electrical field, $\mathbf{E}$, act on the system. As a first approximation it is assumed that the fluid electrical dipole moment per unit mass, $\mathbf{p}_{\mathrm{el}}$, is homogeneous and described by the linear relation

$$\frac{d\mathbf{p}_{\mathrm{el}}}{dt}=\frac{1}{\tau_{\mathrm{el}}}(\alpha\mathbf{E}-\mathbf{p}_{\mathrm{el}}), \tag{24}$$

where τ_{el} is the dipolar relaxation time and α is the polarizability per unit mass of the fluid. In Eq. (24) the contribution from the fluid alignment to the electrical field is ignored and the relation is only strictly valid for sufficiently small electrical field strength. The electrical field exerts a torque on the fluid given by $\mathbf{\Gamma}=\mathbf{p}_{\mathrm{el}}\times\mathbf{E}$. For a stationary electrical field the

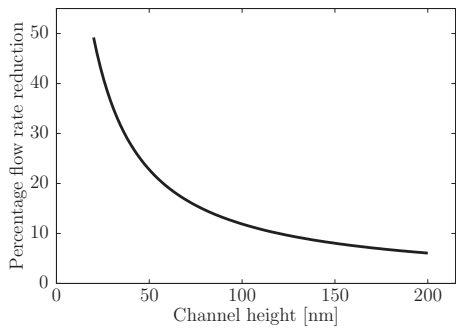

FIG. 3. The rotational viscosity-induced flow rate reduction $1-Q/Q^p$, Eq. (23), vs channel height for Poiseuille flow in a nanoslit. Here $\zeta_0=1.1^{-21}$ kg m s^{-1}, $\zeta_r=1.4\times10^{-21}$ kg m s^{-1}, $\eta_r=1.7\times10^{-4}$ Pa s, and $\eta_0=1\times10^{-3}$ Pa s corresponding to water at $T=298$ K.

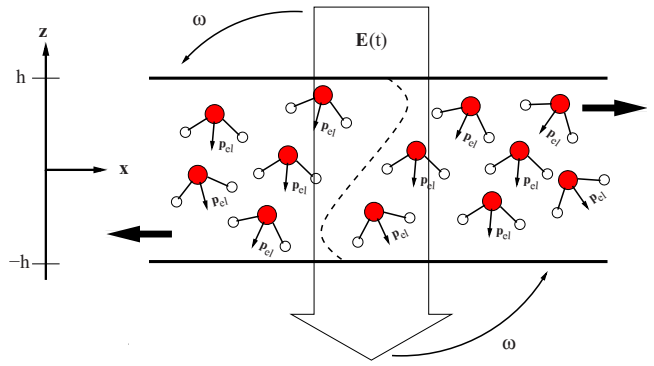

FIG. 4. Illustration of flow generation using a rotating electrical field, $\mathbf{E}(t)$. The water molecules have a permanent electrical dipole, here denoted $\mathbf{p}_{el}$ (which is not perfectly aligned with the field due to thermal fluctuations). The velocity profile is indicated by the dotted line and illustrates the opposite flow directions as shown by the thick black arrows.

torque decays in the order of the dipolar relaxation time, τ_{el}, thus to keep a constant torque we can apply a rotating field in the (x,z)-plane which is relevant for our geometry, i.e., we have

$$\mathbf{E} = (E_x, E_z) = E_0[\cos(\omega t), \sin(\omega t)]. \tag{25}$$

E_0 is the field amplitude. Note that for sufficiently small field strengths, and with $\mathbf{p}_{el}=(p_x,p_z)$, the resulting torque is normal to the (x,z)-plane and we can write this as

$$\Gamma_y = p_z E_x - p_x E_z. \tag{26}$$

Figure 4 shows an illustration of the system.

We assume that one of the walls is coated with a hydrophobic material and the other wall with a hydrophilic material. This will lead to different slip lengths, namely, L_s' and L_s'', respectively, and introduce an average unidirectional mean flow. To study this further the extended Navier–Stokes equations, Eq. (22), have been solved numerically setting $F_e=0$ and by applying the mixed boundary conditions

$$L_s' \left.\frac{\partial u_x}{\partial z}\right|_{z=-h} = -u(-h), \quad L_s'' \left.\frac{\partial u}{\partial z}\right|_{z=+h} = -u(+h)$$

and

$$\Omega_y(\pm h) = 0. \tag{27}$$

The slip length at $z=-h$, L_s' is defined as the z value where tangent line $t(z)=\partial_z u|_{z=-h} z + u(-h)$ crosses the z axis, thus, at the lower boundary $L_s'<0$ for our geometry. Using the same definition for L_s'' means that $L_s''>0$. The classical no-slip boundary condition for Ω_y is based on results from molecular dynamics simulations.[4] Figure 5 shows the resulting velocity and angular velocity profiles for water confined in a nanoslit pore where the field strength is 3.0×10^5 V m^{-1} and where $\omega=200$ MHz. We note that the dielectric breakdown of water is roughly 10×10^6 V m^{-1}.[31] It is seen that due to the different slip lengths a mean unidirectional flow is generated by the rotating field. One can increase the flow by increasing the electrical field or the field frequency. It should be mentioned that the conversion of angular momentum into linear momentum is possible on larger length scales, however, it is a practical problem to obtain sufficiently large electrical field strengths when the pore width increases.

V. CONCLUSION

In this paper we have, for the first time, calculated the rotational viscosity and the spin viscosities for the flexible SPC/Fw water model for different temperatures. It is found that the rotational viscosity is almost independent of temperature in the range 284–319 K, whereas the spin viscosities decrease for increasing temperature. The spin viscosities are orders of magnitude larger than what may be expected from simple scaling laws.[7] This result leads to a significant increase in the effect from the coupling between the angular momentum and linear momentum.

In Fig. 3 we have shown that for a simple planar Poiseuille flow of water in nanoslits, the flow rate reduction is a noticeable 5% already at slit heights of 200 nm, it rises to 15% for a 100 nm channel and increases dramatically to 50% at 20 nm, a channel height that is routinely fabricated today.[32,33] In the nanofluidic community there has been a great deal of focus on the slip boundary condition, which is believed to be the mechanism behind the large flow enhancement of water through carbon nanotubes.[34] While the slip phenomenon is promising in that it indicates that satisfactory flow rates are indeed obtainable in nanochannels, the coupling behavior has the opposite effect. Thus, in order to predict the flow rate accurately, the coupling between the molecular intrinsic angular momentum and the fluid linear momentum must be included for sufficiently small length scales.

It is possible to define a characteristic length as $l=\sqrt{(\zeta_0+\zeta_r)/\eta_0}$. This is a measure of the length scale at which the angular momentum diffusion becomes important compared to the linear momentum diffusion. For water at the state points studied here this characteristic length is around 1.7 nm. We stress that for sufficiently small channel widths (smaller than 3–5 nm), spatial correlations may become important leaving the local constitutive relations given in Eqs. (1) and (2) invalid. Furthermore, for such high degree of

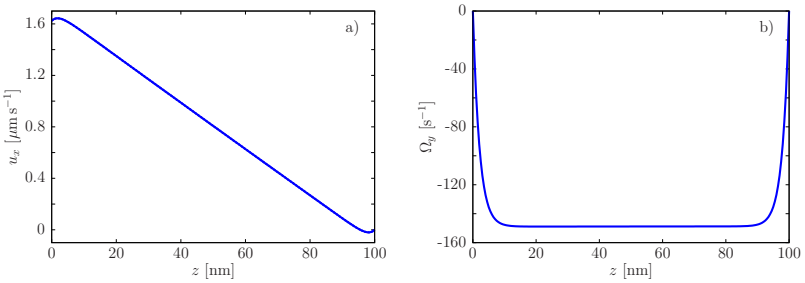

FIG. 5. (a) Calculated streaming velocity profile $u_x(z)$ and (b) angular velocity profile $\Omega_y(z)$ for water confined in a 100 nm nanoslit pore. The electrical field strength is $E_0=3.0\times10^5$ V m^{-1} and rotates with frequency $\omega=200$ MHz. The transport coefficients are the same as in Fig. 3, I is set to 8.4×10^{-22} m^2, $L_s'=-80$ nm and $L_s''=0$ nm (Ref. 30). From Bonthuis *et al.* (Ref. 7) we have used $\tau_{el}=1\times10^{-11}$ s and $\alpha=5.28\times10^{-13}$ (C s/kg)^2.

confinement the system is largely anisotropic. Therefore, in order to correctly predict the flow rate reduction for such a system one would have to treat the four kernels as tensorial quantities due to the anisotropy.

In future molecular dynamics studies of this problem it would be interesting to see how the results are affected by the choice of molecular model, by the way the electrostatic interactions are computed and by change in model parameters.

Also, following Bonthuis *et al.*[7] we showed the coupling can be exploited to generate a unidirectional mean flow. To realize this one needs (i) a fast rotating field $\omega > 100$ MHz, (ii) large field strengths $E_0 > 1 \times 10^5$ V m^{-1}, and (iii) one hydrophobic wall and one hydrophilic wall. Especially, points (i) and (ii) pose some practical challenges. An effective rotational field can be accomplished via a quadrupole, however, it is questionable whether it is possible to realize such high frequencies and field strengths in the laboratory.

[1] M. Born, Z. Phys. **1**, 221 (1920).
[2] H. Grad, Commun. Pure Appl. Math. **5**, 455 (1952).
[3] S. R. de Groot and P. Mazur, *Non-Equilibrium Thermodynamics* (Dover, Mineola, 1984).
[4] J. S. Hansen, B. D. Todd, and P. J. Daivis, Phys. Rev. E **77**, 066707 (2008).
[5] J. S. Hansen, P. J. Daivis, and B. D. Todd, Microfluid Nanofluid **6**, 785 (2009).
[6] J. S. Hansen, P. J. Daivis, and B. D. Todd, Phys. Rev. E **80**, 046322 (2009).
[7] J. D. Bonthuis, D. Horinek, L. Bocquet, and R. R. Netz, Phys. Rev. Lett. **103**, 144503 (2009).
[8] D. J. Evans and W. B. Streett, Mol. Phys. **36**, 161 (1978).
[9] Using the results from Bertolini and Tani (Ref. 27) for the rotational viscosity of water yields roughly $(\zeta_0 + \zeta_r) = 9 \times 10^{-24}$ kg m s^{-1}.
[10] Y. Wu, H. L. Tepper, and G. A. Voth, J. Chem. Phys. **124**, 024503 (2006).
[11] G. Raabe and R. J. Sadus, J. Chem. Phys. **126**, 044701 (2007).
[12] D. Wolf, P. Keblinski, S. R. Phillpot, and J. Eggebrecht, J. Chem. Phys. **110**, 8254 (1999).
[13] D. Zahn, B. Schilling, and S. M. Kast, J. Phys. Chem. B **106**, 10725 (2002).
[14] B. Hess, J. Chem. Phys. **116**, 209 (2002).
[15] *CRC Handbook of Chemistry and Physics*, edited by D. R. Lide (CRC, Cleveland, 1976).
[16] K. Krynicki, C. D. Green, and D. W. Sawyer, Faraday Discuss. Chem. Soc. **66**, 199 (1978).
[17] D. Frenkel and B. Smit, *Understanding Molecular Simulation* (Academic, London, 1996).
[18] S. Nosé, Mol. Phys. **52**, 255 (1984).
[19] W. G. Hoover, Phys. Rev. A **31**, 1695 (1985).
[20] D. J. Evans and H. J. M. Hanley, Phys. Rev. A **25**, 1771 (1982).
[21] B. D. Todd and P. J. Daivis, Mol. Simul. **33**, 189 (2007).
[22] D. J. Evans and G. P. Morriss, *Statistical Mechanics of Nonequilibrium Liquids* (Academic, London, 1990).
[23] Regarding ζ_0, Evans and Streett use a generalization of the Green–Kubo relation that allows the fluxes to be in any arbitrary direction. Notice that the correlation function is given by a double contraction of the couple tensor which is why it is necessary to divide with a factor 10. In this work we have used the standard Green–Kubo formalism with three correlation functions (one for each off-diagonal tensor element), hence the factor of 3. These two expressions are equivalent and produce the same transport coefficients.
[24] Regarding ζ_r, Evans and Streett use the vector dual of the antisymmetric part of the couple tensor. This vector can be found as given in Eq. (12) in our paper. From Eq. (17b) it can be seen that we use the exact same tensor components as Evans and Street [notice their dot product in Eq. (17) in Ref. 8].
[25] M. A. González and J. L. F. Abascal, J. Chem. Phys. **132**, 096101 (2010).
[26] W. H. Press, W. T. Vettering, S. A. Teukolsky, and B. P. Flannery, *Numerical Recipes in C* (Cambridge University Press, Cambridge, 1992).
[27] D. Bertolini and A. Tani, Phys. Rev. E **52**, 1699 (1995).
[28] A. C. Eringen, in *Contribution to Mechanics*, edited by D. Abir (Pergamon, Oxford, 1969).
[29] Hansen *et al.* have written the wrong equation, Eq. (36) in their paper (Ref. 6), but their graph is correct.
[30] J. H. Walther, T. Werder, R. L. Jaffe, and P. Koumoutsakos, Phys. Rev. E **69**, 062201 (2004).
[31] W. A. Stygar, M. E. Savage, T. C. Wagoner, L. F. Bennett, J. P. Corley G. L. Donovan, D. L. Fehl, H. C. Ives, K. R. LeChien, G. T. Leifeste, F. W. Long, R. G. McKee, J. A. Mills, J. K. Moore, J. J. Ramirez, B. S. Stoltzfus, K. W. Struve, and J. R. Woodworth, Phys. Rev. ST Accel. Beams **12**, 010402 (2009).
[32] N. R. Tas, J. Haneveld, H. V. Jansen, M. Elwenspoek, and A. van den Berg, Appl. Phys. Lett. **85**, 3274 (2004).
[33] L. H. Thamdrup, F. Persson, H. Bruus, H. K. Flyvbjerg, and A. Kristensen, Appl. Phys. Lett. **91**, 163505 (2007).
[34] J. A. Thomas and J. H. McGaughey, Nano Lett. **8**, 2788 (2008).